Two-Agent Formation Control of Magnetic Microrobots

Mohammad Salehizadeh
Department of Mechanical and Industrial Engineering
University of Toronto
Ontario, CANADA
Email: msalehi@mie.utoronto.ca

Eric Diller
Department of Mechanical and Industrial Engineering
University of Toronto
Ontario, CANADA
Email: ediller@mie.utoronto.ca

***Abstract*—This paper presents a new method to control multiple micro-scale magnetic agents operating in close proximity to each other for applications in microrobotics. Controlling multiple magnetic microrobots close to each other is difficult due to magnetic interactions between the agents, and here we seek to control those interactions for the creation of desired multi-agent formations. We use the fact that all magnetic agents orient to the global input magnetic field to modulate the local attraction-repulsion forces between nearby agents. Here we study these controlled interaction magnetic forces for agents at a water-air interface and devise two controllers to regulate the inter-agent spacing and heading of the set, for motion in two dimensions. Simulation and experimental demonstrations show the feasibility of the idea and its potential for the completion of complex tasks using teams of microrobots. Average tracking error of less than 73 μm and 14° is accomplished for the regulation of the inter-agent space and the pair heading angle, respectively, for identical disk-shape agents with nominal radius of 500 μm and thickness of 80 μm operating within several body-lengths of each other.**

I. Introduction

Microrobots can effectively access small remote spaces with a wide range of potential applications in drug delivery [1], cell lysis/sorting [2], and micro-assembly/disassembly [3]. The ability to exert independent control over a team of microrobots working together on a task has potential to increase task speed and capability [4]. Among many proposed strategies [5], remote actuation using a magnetic field is a common choice because it can penetrate most materials, remotely generate both forces and torques on magnetic materials, and is easy and safe to generate and manipulate [4], [6]. However, swarm control of magnetic micro-agents remains an open-ended problem as in most actuation systems, all magnetic micro-agents share a global driving magnetic signal. In this way, all agents receive identical control inputs and thus it is difficult to steer independently for complex task completion [7], [8]. Outside the microrobotics field, several approaches to particle assembly have been explored. For instance, fluidic interactions are considered to achieve dynamic self-assembly of magnetized objects such as magnetic disks [9], gears [10], and colloidal asters [11]. These particles rotate at a liquid-air interface with complex behaviors and motions that are not possible with conventional systems, but are limited to two-dimensional (2D) applications. In the microrobotics field, a variety of approaches have been explored: Martel et al. [12] achieved swarm control of bacterial actuators in the human microvasculature trackable by a clinical MRI system. Diller et al. [8] employed geometrically or magnetically distinct microrobots to realize independent control of small teams of magnetic agents. Becker et al. [13] exploited differences in cell population to steer cells to goal positions using ensemble control. Nevertheless, all these studies have been done only for a small number of agents with severe limitations such as a lack of path-following capability.

These studies on magnetic micro-agents are also limited in how close the agents can operate to one another. When they do operate close together, the agents exert large magnetic interaction forces on one another, which results in control instability. Such interactions have been used to attach nearby magnet micro-agents together [14], but have not allowed for independent agent operation in close proximity without coming into contact. Most work in the field of magnetic micro-agents assume that inter-agent magnetic fields are small in comparison with the driving actuation field strength, with the associated requirement that the agents be kept far apart from each other (typically several microrobot body-lengths). This constraint limits the ability of teams of agents from working close together. In Miyashita et al. [15], local magnetic interaction forces are used to create a few stable formations in two dimensions of a set. These formations are modulated by dynamically remagnetizing some of the agents, with promise for controlling sets of up to three agents and limited control over a four-agent set. However, that method is limited to a small set of stable configurations, has no control over the formation orientation, cannot be generalized to microrobots moving in three dimensions, and is only applicable to sets of agents which are each magnetically unique (and so cannot scale up to larger sets of agents).

Here we pursue a more general approach for the dynamic regulation of the inter-agent magnetic forces between nearby microrobots. We model the radial and transverse magnetic forces between these agents, and devise a set of controllers to maintain any desired inter-agent separation and pair heading in the presence of these forces. We show for the first time, the stable motion control of multiple identical magnetic micro-

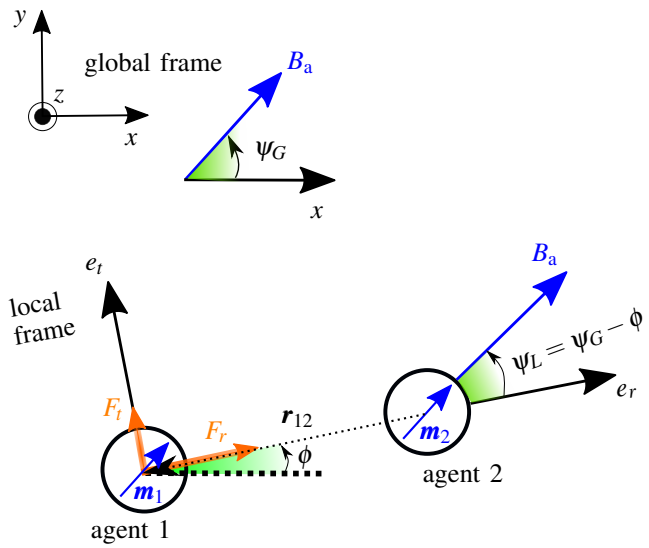

Fig. 1: Pairwise orientation parameters defined in global and local coordinates for agents in close proximity with magnetic moments $\boldsymbol{m}_1$ and $\boldsymbol{m}_2$ aligned with the actuation field $\boldsymbol{B}_a$. $\boldsymbol{r}_{12}$ represents the pairwise distance vector connecting agent 2 to agent 1. $\boldsymbol{F}_r$ and $\boldsymbol{F}_t$ are radial and transverse forces exerted on the first agent by the second agent (corresponding forces acting on agent 2 are not shown).

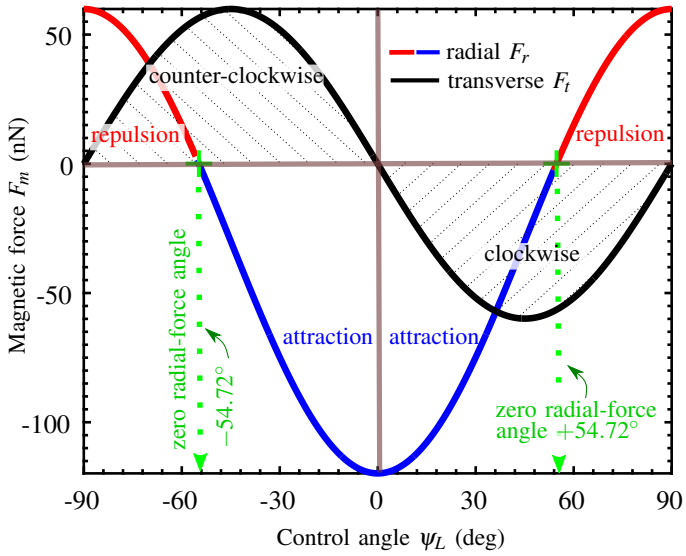

Fig. 2: Inter-agent magnetic force vs. control angle based on eq. (1), for the case of $r = 5R$ (R denotes the radius of agents), $|M| = 10^5$ A/m. The critical angles here include: $\psi_L = 54.72°$ corresponding to the zero-radial force angle, $\psi_L = 0°$ and $\psi_L = \pm 90°$ at which the radial force becomes maximum attractive (negative) and repulsive (positive) value, respectively.

robot agents operating in close proximity. In our design, the spatially-uniform external field creates only torque to orient micro-agents and as a result the inter-agent force appears between agents. We modulate the agents' magnetic moment angle to regulate this force. We choose to make the agents interact at a water-air interface to allow for two-dimensional study.

The paper is structured as follows. Section II describes the kinematics of agents along with the inter-agent force relation. Section III introduces our control principles to regulate the relative motion of agents; accordingly, a systematic feedback control law is synthesized to handle best performance. In Section IV, a simulation based on a physical model is conducted to enable prediction of agents' behaviors; afterwards, fabrication method and experimental setup that is used to control the relative position of agents are presented, then experimental results are carried out. This paper is concluded in Section V.

II. Concepts and Definitions

This section introduces the kinematics describing a pair of agents along with the inter-agent force relation, and lays the foundation for controlling a two-agent configuration.

A. Magnetic actuation and inter-agent kinematics

We base the following analysis on the assumption that the magnetic moment $\boldsymbol{m}$ of all magnetic agents in the workspace align with the applied field $\boldsymbol{B}_a$. We use the angle of the applied field as our control input to the entire system. Consider two identical magnetic agents with magnetic moments $\boldsymbol{m}$ aligned with the uniform external magnetic field $\boldsymbol{B}_a$ applied in the workspace for actuation in a two-dimensional (2D) horizontal plane. As the applied field is uniform over space, no external magnetic forces are generated ($\nabla \boldsymbol{B}_a = 0$). Fig. 1 shows two agents with the relevant kinematic parameterization and interaction forces.

B. Inter-agent magnetic force

We study the forces acting on agent 1 caused by field gradients created by agent 2. The position of agent 1 relative to agent 2 is denoted by $\boldsymbol{r}_{12}$, as depicted in Fig. 1. The magnitude of this vector r_{12} is termed "agent separation" while the angle ϕ made by this vector with the horizontal x-axis is termed "pair heading". We model each agent as a magnetic point dipole and so only consider the magnetic moment in force calculations. Let $\boldsymbol{F}_{12}$ represent the force exerted on the first agent by the second agent as $\boldsymbol{F}_{12} = \nabla(\boldsymbol{m}_1 \cdot \boldsymbol{B}_{12})$, where $\boldsymbol{B}_{12}$ is the magnetic flux density at the position of the first agent with magnetic moment $\boldsymbol{m}_1$ created by the second agent with magnetic moment $\boldsymbol{m}_2$. In local cylindrical coordinates $(\hat{e}_r, \hat{e}_t)$, the radial and transverse components of this local magnetic force can be written as

$$F_r = \frac{-3\mu_0 m_1 m_2}{4\pi r^4}[2cos^2(\psi_L) - sin^2(\psi_L)] \text{ and} \quad (1a)$$

$$F_t = \frac{-3\mu_0 m_1 m_2}{4\pi r^4}[sin(2\psi_L)]. \quad (1b)$$

Here, μ_0 is the permeability of free space, ψ_L the local control input angle defined as the angle between the actuation field $\boldsymbol{B}_a$ and the vector $\boldsymbol{r}_{12}$ as sketched in Fig. 1. Similarly, $\psi_G = \psi_L + \phi$ is the control angle in global coordinates. These force components as a function of control angle are sketched in Fig. 2. From this figure, we can see how to develop a controller for the modulation of the inter-agent magnetic force as a function of the control angle ψ_L. At $\psi_L = 0°$ and $\psi_L = \pm 90°$

the radial force attains its maximum attractive (negative) and repulsive (positive) value, respectively. It is to be noted that the magnitude of the attractive force is roughly twice as large as that of the repulsive force. Importantly, as shown in Fig. 2, at $\psi_L = 54.72^\circ$ the radial force becomes zero. Also, at any angle between 0 and 90°, a non-zero transverse force occurs which causes the pair of agents to rotate about one another. The transverse force peaks at 45°. Additionally, it can be seen from the figure that the radial and transverse forces are even and odd functions of the control angle about 0°, respectively. In other words, by reflecting the control angle about $\psi_L = 0^\circ$, the transverse force can be reversed without affecting the radial force. This reflection will be used to control the pair heading.

C. Input field strength requirement

The total field at the location of an agent is the vector sum of the inter-agent field $\boldsymbol{B}_{12}$ (field on agent 1 created by agent 2) and the actuation field $\boldsymbol{B}_a$. It is convenient to assume that the global field $\boldsymbol{B}_a$ dominates the local field such that all agents always align with the actuation field. Here we check our assumption that the local field created by a nearby agent does not rotate the total field at an agent's location. To avoid this phenomenon, the actuation field strength can be chosen to keep the total field angle error less than a threshold given by $\theta_e = \psi_a - \psi_L$, where ψ_a represents the angle of total field. For a given angle error threshold θ_e, the minimum required field strength $B_{\min}$ is

$$B_{\min} = \frac{-\mu_0 m}{4\pi r^3}\left[\frac{2\tan(\theta_e+\psi_L)+\tan(\psi_L)}{\tan(\psi_L)-\tan(\theta_e+\psi_L)}\right]. \quad (2)$$

Fig. 3 shows the minimum required field strength as a function of agent separation r for multiple control angle inputs, using a maximum angle error of $\theta_e = 5^\circ$. It is noted that $\psi_L = 0$ and $\psi_L = 90^\circ$ see no angle error as the local and global fields are parallel in these cases. To ensure that the agents align to the applied field, the minimum field strength is applied. For the experimental section of this paper, agent spacing is roughly $5R$, so we maintain a field strength of 2 mT to be higher than the minimum required and assume that the agents always align with $\boldsymbol{B}_a$.

D. Other forces

1) Fluid drag force: The microrobots used in this study are 500 μm in radius and 80 μm in thickness, and are experiencing low Reynolds number fluid flow. Therefore, a first-order model is considered to describe the agents' motion based on the Stokes fluid drag model as

$$\dot{\boldsymbol{x}} = -\frac{\boldsymbol{F}_m}{b}, \quad (3)$$

where $\dot{\boldsymbol{x}}$ is the induced agent velocity and $\boldsymbol{F_m}$ is the inter-agent magnetic force. The term $b = 6\pi\mu R$, fluid drag constant, depends on liquid viscosity, μ, and the radius of the assumed spherical agents, R.

2) Capillary force: In this work, we restrict the agents to operate at a water-air interface to constrain their motion to two dimensions, and assume that the Stokes fluid drag model still holds. The agents stay suspended at the interface by capillary forces. Depending on the materials used for the agents and the liquid container, horizontal capillary forces between agents and between the container and the agents may exist [9]. Our estimation shows these forces have a magnitude 100 times less than the magnetic force; in other words, the observation meets our assumption that the capillary force impact is negligible against the magnetic force at the operating separation range for a water-air interface.

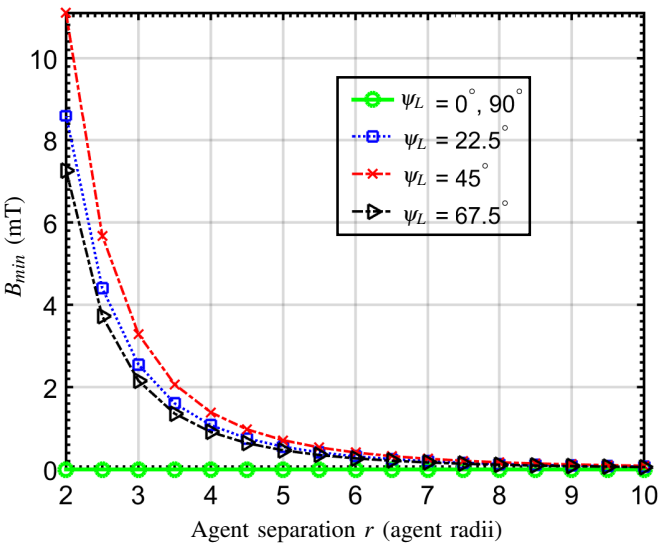

Fig. 3: Minimum required input field strength as a function of agent separation r for multiple control angles to limit the total angle error to $\theta_e = 5^\circ$ ($|M| = 10^5$ A/m).

III. Control of Two-Agent Configuration

This section presents our approach to regulate the agent separation and pair heading angle. The task in designing a controller is to choose the input magnetic field angle ψ_L to push the relative spacing and angle of the pair towards the goal state. The basis for producing these radial and transverse forces is shown in Fig. 4(a). We start with the simplest radial controller with two input states, then generalize to a proportional radial controller. Finally we introduce a transverse angle controller.

A. Radial (separation) controller

1) Bang-Bang control principle: The simplest radial controller has two states as illustrated in Fig. 4(a) (i-ii). These two states lead to repulsion or attraction of the two agents, when their moments are perpendicular or parallel to their separation vector, respectively.

(i) If the space between two agents is too small ($r < r_{des}$), the controller points the field orientation perpendicular to their separation vector $\boldsymbol{r}$ so that the agents repel each other with full radial force. This is done by applying $\psi_L = 90^\circ$. The transverse force at $\psi_L = 90^\circ$ is zero.

(ii) If the space between two agents is too large ($r > r_{des}$), the controller points the field orientation parallel to their

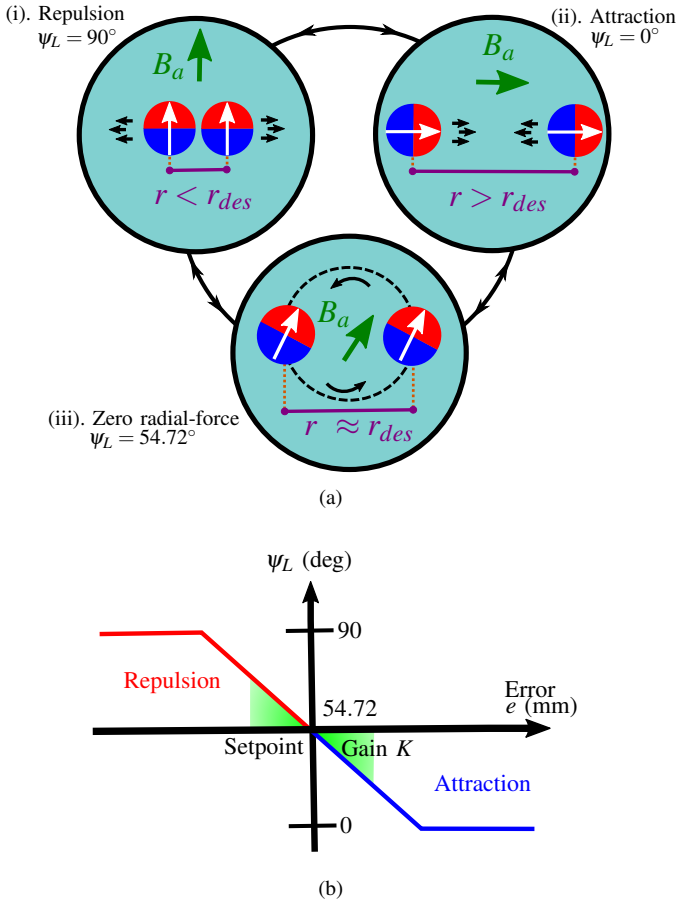

Fig. 4: Two-agent configuration control principle. (a) States of agent attraction or repulsion are determined by the direction of applied field $\boldsymbol{B}_a$: i) repulsion at $\psi_L = 90°$, ii) attraction at $\psi_L = 0°$, iii) zero radial-force at $\psi_L = 54.72°$. (b) Radial proportional controller design.

separation vector $\boldsymbol{r}$ so that the agents attract each other with full radial force. This is done by applying $\psi_L = 0°$. The transverse force at $\psi_L = 0°$ is zero.

(iii) (optional) If the space between two agents is close to the goal spacing ($r \approx r_{des}$), the control angle is set to $\psi_L = 54.72°$ such that the radial force is zero. In this state, a transverse force is created which rotates the pair (we ignore this rotation for now).

2) Proportional control: The bang-bang controller suffers from a low level of precision due to its binary input states. A more sophisticated controller would choose intermediate angles between those shown in Fig. 4(b), centered around the zero-radial force angle. To create a proportional controller (P-controller), we define the radial separation error $e = r - r_{des}$, which allows us to give the proportional control law as $\psi_L = \psi_s - K\|e\|$. Thus, the controller applies a larger radial force correction for larger separation errors e (up to saturation) as shown in Fig. 4(b). The gain K is tuned manually to result in a stable controller with good performance. It can be noted that the Bang-Bang control law is a special case of the radial P-controller with infinite gain K.

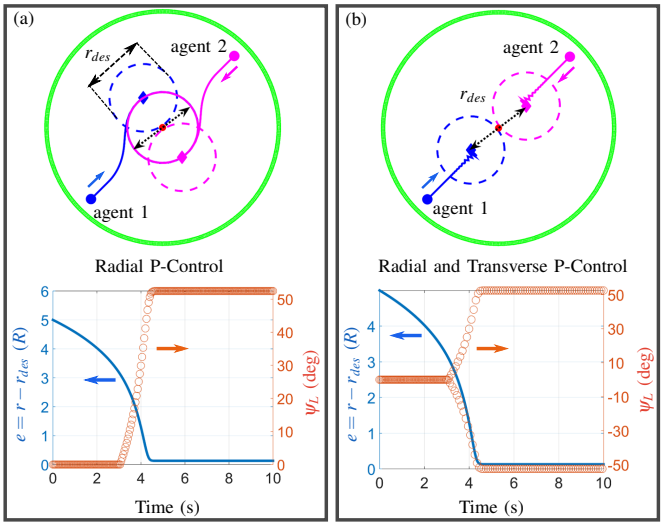

Fig. 5: Two-agent configuration control simulation. (a) Radial P-control. (b) Radial and transverse P-control (R denotes the radius of agents equal to 500 μm). The top plots show the motion trajectory simulation associated to each controller in solid line. The desired pairwise separation r_{des} is reached when the sketched surrounding dashed-line circles around agents with radius equal to $r_{des}/2$ come into contact with one another. Initial positions are denoted by circle and current position with diamond. Here the initial separation is $r = 10R$ assuming the desired separation to be $r_{des} = 5R$, and $|M| = 10^5$ A/m. The bottom graphs illustrate the separation error and control angle input as a function of time for each controller.

B. Angle (pair heading) control

For control angle inputs between $\psi_L = 0°$ or 90°, a transverse force F_t will be induced on the agents according to eq. (1b). If we wish to control the pair heading, we can choose the sign of this transverse force by choosing whether we operate with positive or negative values of ψ_L as shown in Fig. 2. Because F_r is symmetric about $\psi_L = 0°$, reversing the sign of ψ_L does not affect the radial controller already introduced. Although we cannot arbitrarily choose desired values of both F_r and F_t, we can regulate the radial force proportionally while introducing a bang-bang type binary controller on the transverse force. We choose to keep the proportional controller on the radial rather than the transverse force because this coordinate tends to be unstable (due to the r^{-4} relationship on F_r in eq. (1a)). Using this scheme, the control of the two parameters r and ϕ can be regulated using a single magnetic global input. In the next section, the effectiveness of this control method is characterized.

IV. Results

This section presents numerical simulation results, the fabrication process and experimental setups, and the experimental results of the proposed controller for two-agent configuration.

A. Simulation

Fig. 5 shows numerical simulation of the motion trajectory of magnetic agents in two-agent configuration using the P-controller in two modes: (a) radial P-control, (b) radial and

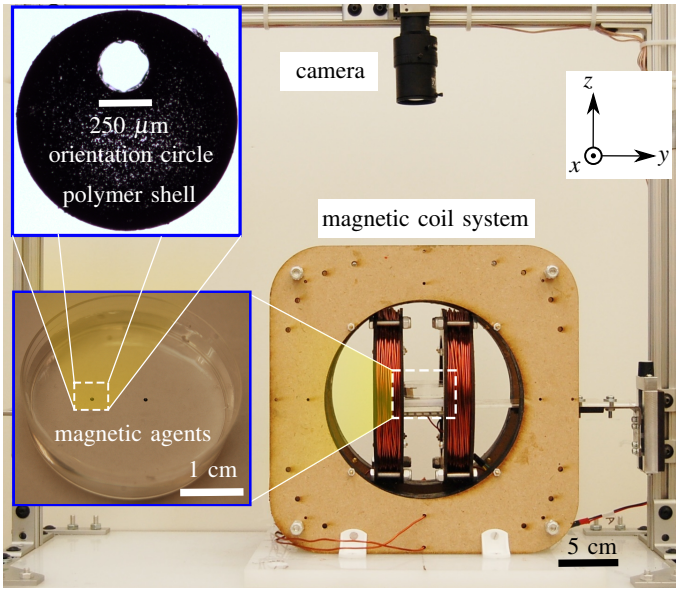

Fig. 6: Experimental setup. In the inset image of agent, the orientation circle atop mimics the north side of each agent's magnetic moment. The identical disk-shape agents shown have a radius of 500 μm and thickness of 80 μm that float on water surface. The agents are driven in horizontal plane by an electromagnetic coil system with two pairs of coils capable of producing fields in the $x-y$ plane.

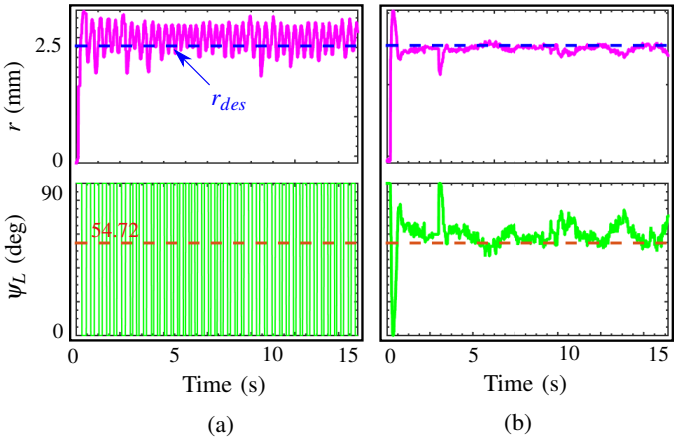

Fig. 7: Experimental results comparing (a) Bang-Bang, and (b) radial (no transverse) P-controller. Experiments are done using magnetic field strength of $|\boldsymbol{B}_a| = 2$ mT and gain $K = 2$ (deg/mm) to reach the desired separation of $r_{des} = 2.5$ mm. Radial P-controller with separation tracking RMS error of 130 μm has a more stable performance compared with Bang-Bang with separation tracking error of 197 μm. Also in P-controller the input angle ψ_L varies about the zero-radial force angle instead of aggressively jumping between 0° and 90° in Bang-Bang (multimedia is available at [17]).

transverse P-control. This simulation is a time integration of eq. (1) for initial condition of $r = 10R$ and parameters $|M| = 10^5$ A/m, $\mu = 8.9 \times 10^{-4}$ Pa s. Although the agents have a disk shape, for simplification we model them as spheres to calculate the fluid drag force eq. (3). The inter-agent and agent-air-wall capillary forces, as well as inertial forces are ignored in the simulation. The simulation shows a particular case where two agents are initially far away ($r = 10$R). It can be seen that both controllers approach the goal configuration and the error reduces to a small value over time. We have seen in simulation that the controllers are stable for a wide variety of initial conditions.

B. Fabrication of agents and experimental setup

Magnetic agents are fabricated as in Zhang and Diller [16]. We describe briefly the fabrication process involving: (a) making mold using photolithography, (b) pouring polymer and curing toward desired shape. Identical agents are composed of magnetic microparticles mixed with polyurethane polymer (BJB M-3184), which is poured into a negative mold to define the agent shape, degassed in a vacuum pump and scraped level using a razor blade. The mold is made using SU-8 photolithography and a replica molding process. Magnetic fields for agent actuation are created in an electromagnetic coil system with two pairs of coils nested orthogonally to create fields in the plane, powered by two analog servo drives (30A8, Advanced Motion Controls). Each pair of wire loops in the coil system is arranged in Helmholtz configuration, resulting in a uniform magnetic field up to 15 mT (uniform to within 5% of nominal at the center over a workspace size of 5 cm) located at center of the coil system (see Fig. 6). The strength of magnetic field is smaller than the coercivity of the magnetic materials in the agent, and so the agents' magnetization will not be altered by the actuation field. Agent position is detected using a camera (FO134TC, FOculus) mounted atop the workspace, and a computer with custom C++ code finds agent positions using a Hough Circle Transform in the openCV library at 60 frames/second [16]. Two identical agents are placed in a plastic petri dish on water as illustrated in Fig. 6.

C. Experiment

We tested two types of controllers:

1) Radial (no transverse) control: Fig. 7 shows the experimental results for (a) Bang-Bang, and (b) radial (no transverse) P-control. While both controllers demonstrate asymptotic stability during this experiment, the P-controller achieves a lower RMS error from the goal of 130 μm as compared with 197 μm for the Bang-Bang controller. The control angle signal in Fig. 7(b) demonstrates that the attraction force tends to be greater in magnitude than the repulsion force in pulling the agents toward each other, as the inter-agent attractive force is stronger than the inter-agent repulsive force (as discussed in Section II-B). As aforementioned, in Bang-Bang the control input can take only two states of $\psi_L = 0°$ and 90°. However, during the experiment (multimedia is available at [17]), agents' moments physically sweep through the continuous range of local angles between 0° and 90°, although this leads to a negligible impact on stability. In addition, a slight displacement of the pair of agents is observed due to other disturbance forces potentially the one resulted from small non-uniformity of the actuation field. It is to be noted that one can not use Bang-Bang to control the transverse motion, because at the possible input angles the transverse force will be always zero.

2) Radial and transverse control together: Fig. 8 shows the experimental results for separation and pair heading control

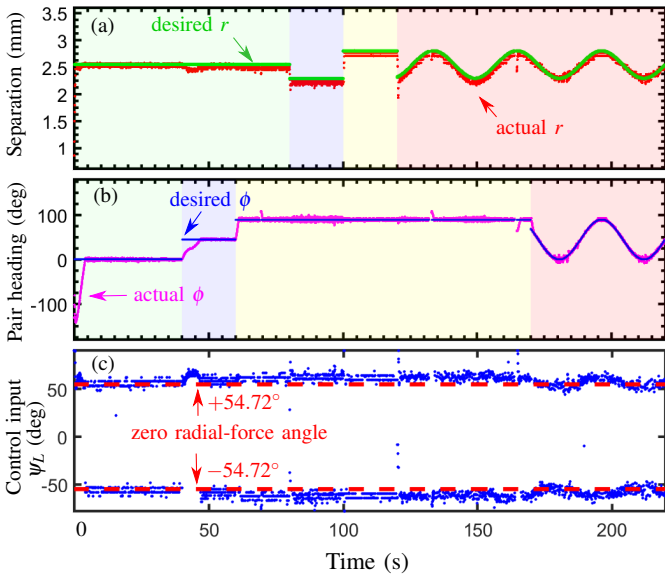

Fig. 8: (a) Separation r and (b) pair heading ϕ tracking using radial and transverse P-controller together along with (c) the applied control angle input ψ_L. The control angle flips to maintain the desired pair heading angle. RMS tracking error of less than 73 μm and 14° is accomplished for the regulation of the separation and the pair heading angle, respectively (multimedia is available at [17]).

to track a changing goal state. RMS tracking error of less than 73 μm and 14° is accomplished for the regulation of the separation and the pair heading angle, respectively. Although tracking is achieved, there is a small undesired coupling between the controllers. Ideally, to be able to independently control r and ϕ, flipping the control angle for transverse control needs to occur instantaneously. One can confirm by tracking the agent orientation in the video [17], that the agents remain aligned with the actuation field during the entire experiment. However, the agents take approximately 100 ms to align with the field when it switches direction suddenly. Also, as mentioned earlier, for a rotating actuation field with a constant strength, if the separation between agents becomes too small, not only angle error interference may come to play, but also the appeared local force is hard to overcome by a general controller.

V. Conclusions

In this paper, for the first time, a method was introduced to control the motion of small-scale identical magnetic robots in close proximity with each other. This paper established a tool for multi-agent control of magnetic microrobots using a global magnetic field. We designed a set of controllers to maintain any inter-agent separation and pair heading in two dimensions (2D) via modulation of the inter-agent magnetic force. Simulation and experimental results showed precise tracking with two magnetic agents along various combinations of the separation and pair heading trajectories. For the controller to operate without instability, the relative spacing between agents in this work needed to be between 3 and 30 agent's radius. Future work will widen this range by using larger applied fields and faster controllers. Fluid and capillary interactions were assumed to be negligible in this study. However, it is recommended to tailor these forces for various liquid interfaces. In future work, the proposed scheme will be extended to 3D and agent pair formation will be examined using field gradient under liquid surface taking into account gravity. Future research will investigate the problem of manipulating multiple agents to complete useful tasks using a team of agents in 3D fluidic environments.

References

[1] B. J. Nelson, I. K. Kaliakatsos, and J. J. Abbott, "Microrobots for minimally invasive medicine," *Annual Review of Biomedical Engineering*, vol. 12, pp. 55–85, 2010.

[2] E. B. Steager, M. S. Sakar, C. Magee, M. Kennedy, A. Cowley, and V. Kumar, "Automated biomanipulation of single cells using magnetic microrobots," *The International Journal of Robotics Research*, vol. 32, no. 3, pp. 346–359, 2013.

[3] G. M. Whitesides and B. Grzybowski, "Self-assembly at all scales," *Science*, vol. 295, no. 5564, pp. 2418–2421, 2002.

[4] E. Diller and M. Sitti, "Three-dimensional programmable assembly by untethered magnetic robotic micro-grippers," *Advanced Functional Materials*, vol. 24, no. 28, pp. 4397–4404, 2014.

[5] W. Hu, Q. Fan, and A. T. Ohta, "Interactive actuation of multiple opto-thermocapillary flow-addressed bubble microrobots," *Robotics and Biomimetics*, vol. 1, no. 1, pp. 1–6, 2014.

[6] J. J. Abbott, M. C. Lagomarsino, L. Zhang, L. Dong, and B. J. Nelson, "How should microrobots swim?" *The International Journal of Robotics Research*, vol. 28, no. 11-12, pp. 1434–1447, 2009.

[7] S. Chowdhury, W. Jing, and D. J. Cappelleri, "Controlling multiple microrobots: recent progress and future challenges," *Journal of Micro-Bio Robotics*, vol. 10, no. 1-4, pp. 1–11, 2015.

[8] E. Diller, J. Giltinan, and M. Sitti, "Independent control of multiple magnetic microrobots in three dimensions," *The International Journal of Robotics Research*, vol. 32, no. 5, pp. 614–631, 2013.

[9] J. M. Ng, M. J. Fuerstman, B. A. Grzybowski, H. A. Stone, and G. M. Whitesides, "Self-assembly of gears at a fluid/air interface," *Journal of the American Chemical Society*, vol. 125, no. 26, pp. 7948–7958, 2003.

[10] B. A. Grzybowski, H. A. Stone, and G. M. Whitesides, "Dynamic self-assembly of magnetized, millimetre-sized objects rotating at a liquid–air interface," *Nature*, vol. 405, no. 6790, pp. 1033–1036, 2000.

[11] A. Snezhko and I. S. Aranson, "Magnetic manipulation of self-assembled colloidal asters," *Nature Materials*, vol. 10, no. 9, pp. 698–703, 2011.

[12] S. Martel, M. Mohammadi, O. Felfoul, Z. Lu, and P. Pouponneau, "Flagellated magnetotactic bacteria as controlled mri-trackable propulsion and steering systems for medical nanorobots operating in the human microvasculature," *The International Journal of Robotics Research*, vol. 28, no. 4, pp. 571–582, 2009.

[13] A. Becker, Y. Ou, P. Kim, M. J. Kim, and A. Julius, "Feedback control of many magnetized: Tetrahymena pyriformis cells by exploiting phase inhomogeneity," in *IEEE International Conference on Intelligent Robots and Systems*, 2013, pp. 3317–3323.

[14] E. Diller, C. Pawashe, S. Floyd, and M. Sitti, "Assembly and disassembly of magnetic mobile micro-robots towards deterministic 2-D reconfigurable micro-systems," *The International Journal of Robotics Research*, vol. 30, no. 14, pp. 1667–1680, 2011.

[15] S. Miyashita, E. Diller, and M. Sitti, "Two-dimensional magnetic micromodule reconfigurations based on inter-modular interactions," *The International Journal of Robotics Research*, vol. 32, no. 5, pp. 591–613, 2013.

[16] J. Zhang and E. Diller, "Millimeter-scale magnetic swimmers using elastomeric undulations," in *IEEE International Conference on Intelligent Robots and Systems*, 2015, pp. 1706–1711.

[17] Experiment multimedia available online: http://microrobotics.mie.utoronto.ca/?p=474.